Supporting Information

Nonflammable Electrolytes for Lithium Ion Batteries Enabled by Ultraconformal Passivation Interphases

Xia Cao,[†] Yaobin Xu,[‡] Linchao Zhang,[†,§] Mark H. Engelhard,[‡] Lirong Zhong,[†] Xiaodi Ren,[†] Haiping Jia,[†] Bin Liu,[†] Chaojiang Niu,[†] Bethany E. Matthews,[‡] Haiping Wu,[†] Bruce W. Arey,[‡] Chongmin Wang,[‡] Ji-Guang Zhang[,†] and Wu Xu*[,†]*

[†] Energy and Environment Directorate, Pacific Northwest National Laboratory, Richland, Washington 99354, United States

[‡] Environmental Molecular Sciences Laboratory, Pacific Northwest National Laboratory, Richland, Washington 99354, United States

[§] Key Laboratory of Materials Physics, Institute of Solid State Physics, Chinese Academy of Sciences, Hefei, Anhui 230026, China

Corresponding Authors

* E-mail: wu.xu@pnnl.gov (W. X.)

* E-mail: jiguang.zhang@pnnl.gov (J.-G. Z.)

Experimental Methods

Electrolyte and electrode preparation

The electrolytes were prepared by dissolving the LiFSI or $LiPF_6$ in the selected solvent and additive mixtures inside an MBraun glovebox filled with purified argon (Ar), where the moisture and oxygen content was less than 1 ppm. The NMC811 cathode was composed of 96 wt.% NMC811 (Targray, Kirkland, Canada) as active material, 2 wt.% Super C65 as conductive carbon, and 2 wt.% PVDF as binder and had an areal capacity loading of 1.5 mAh cm^{-2}, which was prepared at the Advanced Battery Facility (ABF) at Pacific Northwest National Laboratory. The Gr anode composed of 89.8 wt.% CGR-A12 active graphite, 4 wt.% Super P Li as conductive carbon, 6 wt.% Kureha 9300 as binder and 0.2% oxalic acid additive with an areal capacity loading of 2.0 mAh cm^{-2}, which was obtained from Cell Analysis, Modeling and Prototyping (CAMP) Facility at Argonne National Laboratory. The cathode was punched into 1.27 cm^2 disks and the Gr anode was punched into 2.00 cm^2. The electrode disks were further dried at 120 °C overnight under vacuum before use.

Flammability Tests

The flammability of the five electrolytes studied in this work was tested according to the method reported by Xu et al. [1] 100 µL electrolyte was absorbed in the glass fiber and was ignited for 5 s and leave for a self-extinguish. The self-extinguish time (SET) was calculated by dividing the burning time to the electrolyte weight.

Viscosity tests

Viscosity of the electrolytes as a function of temperature was measured with an Anton Paar rheometer (Ashland, VA, USA). A DG26.7 SS measuring system coupled with a C-PTD200 cell was used. A Peltier system installed in the measuring system was employed for temperature control. A nitrogen flow through the measuring system was established to minimize the sample exposure to air. Before sample loading, the system was flushed with nitrogen. The temperature of electrolyte samples was initially set at -10˚C to start the measurements. Once a measurement was started, temperature was increased linearly in time from -10˚C to 60˚C in a time interval of 40 min while the viscosity was measured and recorded with the values logged in every 15 sec. Shear rate of 60 1/s was used for all measurements.

Electrochemical tests

Electrolyte conductivities were performed on a Bio-Logic MCS 10 fully integrated multichannel conductivity spectroscopy in the temperature range of -10 to 60 °C. CR2032 coin cells (from MTI Corporation) were assembled for electrochemical test. In Li||Gr cells, a piece of Gr anode disk, a piece of polyethylene separator (Asahi Hi-Pore, Japan), and a Li chip (450 µm thick, 1.50 cm diameter, MTI) were sandwiched together with 75 µL electrolyte inside the Ar-filled glovebox. Li||Gr half cells were conducted at C/10 with a cutoff voltage range of 0.01-1.2 V, where 1C rate was 370 mAh g^{-1} on the weight basis of the Gr active material. Gr||NMC811 cells were assembled in the same way with NMC811 as cathode and Gr as anode. The cells were cycled at C/2 charge and 1C discharge rate after two formation cycles at C/20 with a cutoff voltage range of 2.8-4.3 V, where 1 C was 200 mAh g^{-1} on the weight basis of the NMC811 active material.

Characterizations

For postmortem analyses, including SEM, TEM and XPS measurements, the cycled cells were carefully disassembled inside the glovebox to collect the Gr anodes and NMC811 cathodes. These cycled electrodes were rinsed with pure anhydrous EMC solvent to remove residual electrolyte, dried and then sealed in the glovebox before being transferred for characterizations. SEM measurements were carried out on a Helios focused ion beam (FIB)-SEM at an accelerating voltage of 5 kV and a current of 86 pA. The cathode TEM samples were performed on FEI Helios Dual Beam system. A randomly selected secondary particle of NMC811 was coated with a ~2 μm Pt layer. The particle was then extracted along with the capping layers and welded to the TEM grid[2]. The FIB processes were performed at 30 kV, 5 kV and 2 kV to remove the damaged layers and polish the surface[2]. Copper TEM grids (200 mesh, Tedpella, Inc.) were used to prepare the graphite samples by drop casting method in an Ar filled glovebox. The as-prepared samples were characterized by a FEI Titan monochromated (scanning) transmission electron microscope ((S)TEM) equipped with a probe aberration corrector at 300 kV[2-3]. XPS measurements were conducted on a Physical Electronics Quantera scanning X-ray microprobe with a focused monochromatic Al Kα X-ray (1,486.7 eV) source for excitation and a pass energy of 69.0 eV for high-energy-resolution spectra collection.

Table S1. The SET values of five investigated electrolytes.

Electrolyte	**SET / s g^{-1}**	**Flammability**
1 M $LiPF_6$/EC-EMC (3:7 by wt.) (control)	50	Highly flammable
control + 10 wt.% TEPa	25	Flame retardant
control + 10 wt.% TEPa + 2 wt.% VC	33	Flame retardant
1.2 M LiFSI/TEPa-BTFE (LiFSI-1.33TEPa-3BTFE, by mol.)	0	Nonflammable
1.2 M LiFSI/TEPa-EC-BTFE (LiFSI-TEPa-0.3EC-3BTFE, by mol.)	0	Nonflammable

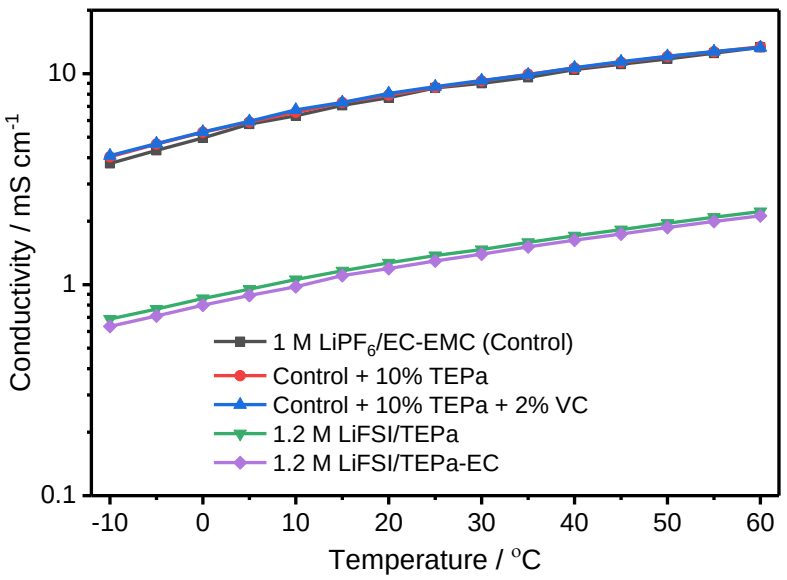

Figure S1. Ionic conductivity of the five investigated electrolytes from -10 to 60 °C.

The three $LiPF_6$/carbonate electrolytes show similar ionic conductivities with temperature, while the two nonflammable LHCEs also show close ionic conductivities in the testing temperature range. The LHCEs have the conductivity values roughly 5 times lower than the $LiPF_6$/carbonate electrolytes, for instance, the ionic conductivities at 30 °C are ca 1.4 mS cm^{-1} for LHCEs while ca. 8.6 mS cm^{-1} for carbonate electrolytes.

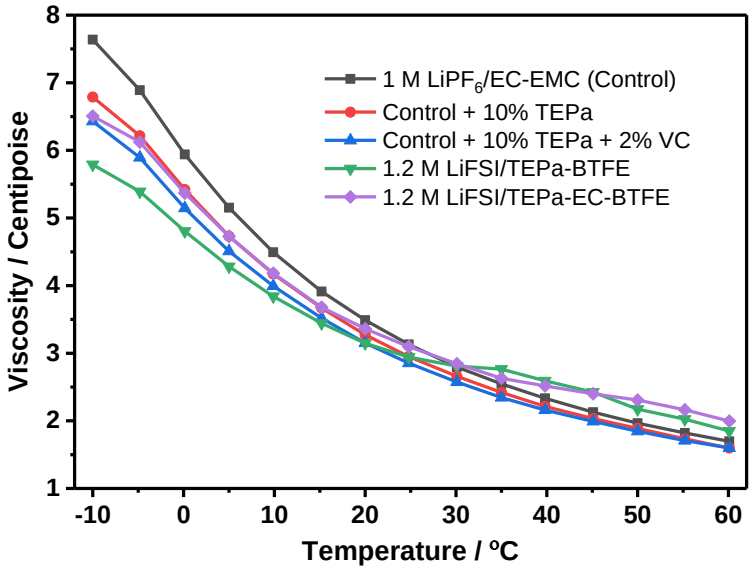

Figure S2. Viscosity of the five investigated electrolytes from -10 to 60 °C.

As shown in Figure S2, the viscosities of these five electrolytes are very close. For example, the viscosity value at 30 °C is in range of 2.5-2.8 cP. On the other hand, the viscosity of the LHCEs is less influenced than the $LiPF_6$/carbonate electrolytes in the studied temperature change.

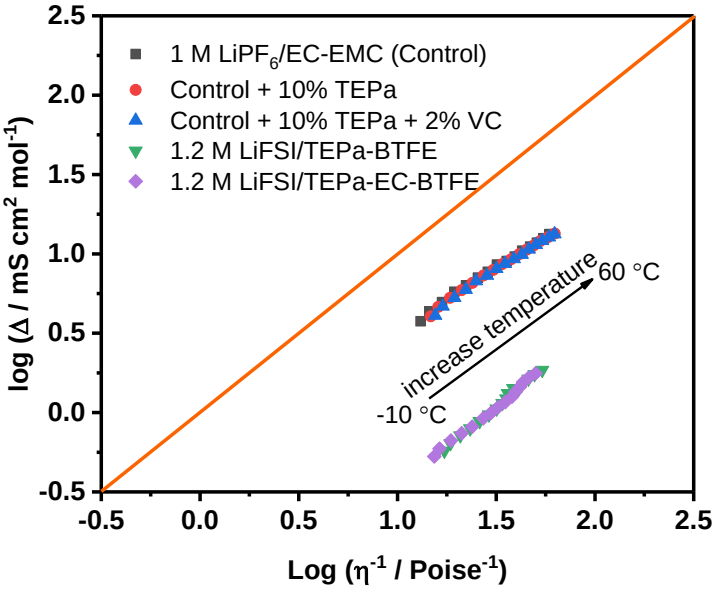

Figure S3. Walden plot of the five electrolytes according to the conductivity and viscosity with temperature.

By combining the conductivity and viscosity data, the Walden plots of the five electrolytes were calculated and are shown in Figure S3. Apparently much stronger ion associations are observed in the two LHCEs than the three $LiPF_6$/carbonate electrolytes, which could be explained by the presence of LiFSI-TEPa, LiFSI-EC and/or LiFSI-TEPa-EC solvation complexes in the LHCE electrolytes due to the insolubility of LiFSI in BTFE but the miscibility of TEPa and BTFE, leading to the maintenance of the clusters only existed in the high concentration electrolytes.[4] Without the abundant free solvent molecules to co-ordinate the Li^+ and FSI^- ions as in the conventional $LiPF_6$/carbonate electrolytes, Li^+ cations and FSI^- anions in LHCEs are likely to show stronger bindings with each other. Moreover, the solvation complexes LiFSI-TEPa, LiFSI-EC and/or LiFSI-TEPa-EC are separated by non-solvating fluorinated ether BTFE molecules, [4-5] thus even

stronger ion associations can be formed in the LHCEs because of the reduced electrostatic interactions with other ions as in the concentrated electrolytes. [6]

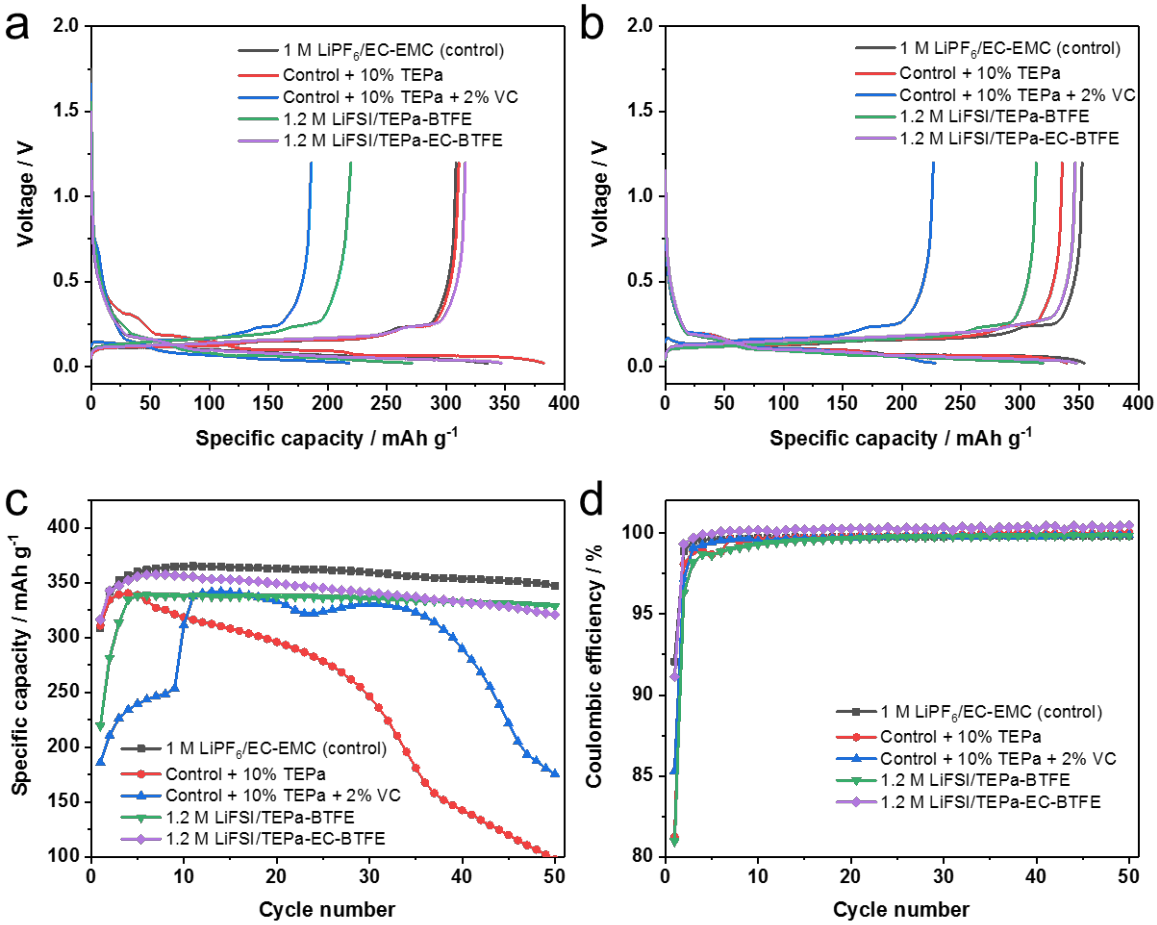

Figure S4. Electrochemical performance of studied electrolytes in Li||Gr cells. (a) First cycle charge/discharge voltage curves at C/20, (b) 3rd cycle charge/discharge voltage curves at C/20, (c) cycling capacity for Li^+ de-intercalation and (d) CE of the Li||Gr cells in the investigated electrolytes, where the Li||Gr cells were cycled at C/20 with the cutoff voltage range of 0.01-1.2 V and 1C = 370 mAh g^{-1} based on the weight of the Gr active material.

For the Li||Gr cells, as shown in Figure S4a, the control electrolyte starts to reduce at ca. 0.8 V, which is related to the EC decomposition and SEI formation on the Gr anode. [7] The formed SEI thereafter protects the Gr anode and enables a stable cycling of Gr anode as shown in Figure S4c and S4d. The cell shows an initial specific capacity of 308.6 mAh g^{-1} and CE of 92.1%. When 10%

TEPa is added into the control electrolyte to form the flame retardant electrolyte, an additional plateau at about 0.3 V is observed as the red line in Figure S4a, which can be attributed to the co-intercalation of the TEPa into the Gr. This solvent co-intercalation damages the Gr layered structure and results in poor cycling stability as shown in Figure S4c. By adding a film-forming additive VC, the co-intercalation of the TEPa is suppressed because VC forms a more robust protective layer on Gr earlier than the TEPa intercalation. However, as shown in Figure S4a and S4c, the overpotential of the cell increases with the addition of VC. Therefore, the Li^+ intercalation into Gr is not fully completed when the cell reaches the cutoff voltage at 0.01 V, which leads to a much lower capacity than the control electrolyte. The capacity of the cell with the electrolyte of control + TEPa + VC increases in the first 12 cycles (Figure S4c), which is likely due to the increased conductivity of the SEI on Gr over cycling in this electrolyte system. However, fast capacity decay takes place after 40 cycles, showing a similar fading rate as the electrolyte without VC (i.e. control + TEPa), which is possibly caused by the fully consumption of VC. As for the nonflammable LHCE 1.2 M LiFSI/TEPa-BTFE, an initial capacity of 219.6 mAh g^{-1} and an initial CE of 81.0% are obtained in the Li||Gr cell (Figure S4a), which are also lower than those of the control electrolyte. However, the capacity and CE are increased after the two formation cycles (Figure S4b). With the modification of this LHCE by using EC to replace partial TEPa (yield 1.2 M LiFSI/TEPa-EC-BTFE), comparable Li||Gr performance like for the control electrolyte is achieved, showing roughly similar specific capacity and an initial CE of 91.1% (Figure S4a,b). It should be noticed that the capacity fading in Figure S4c may also be related to the side reactions of the electrolyte with Li metal on Li anode side. The CEs of the five investigated electrolytes during the cycling shown in Figure S5d demonstrate that the modified LHCE 1.2 M LiFSI/TEPa-EC-BTFE electrolyte has the highest CE close to 100% over the cycling.

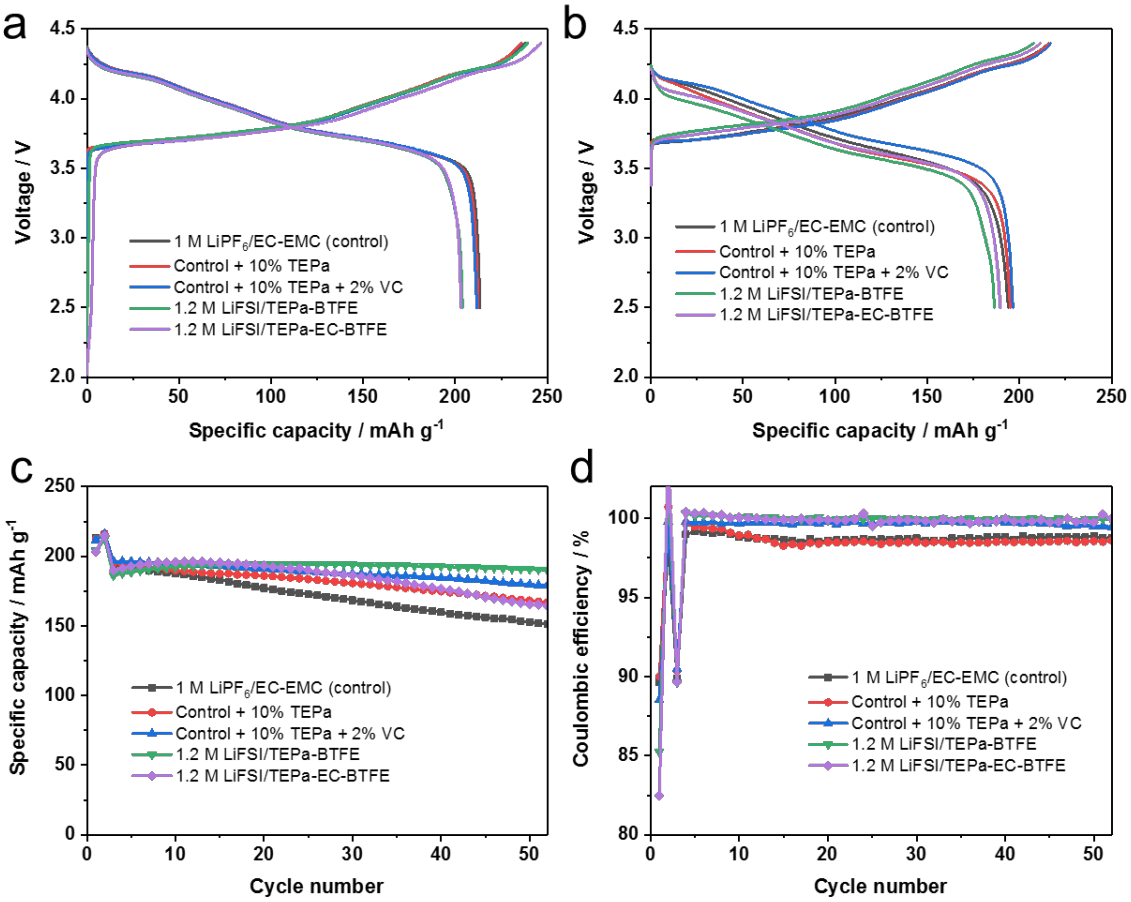

Figure S5. Electrochemical performance of studied electrolytes in Li||NMC811 half cells. (a) First formation charge/discharge voltage curves at C/20, (b) 3rd cycle charge/discharge voltage curves at C/2 charge and 1C discharge, (c) cycling capacity and (d) CE of the Li||NMC811 cells with the investigated electrolytes, where the Li||NMC811 cells were subjected to two formation cycles at C/20 and then cycled at C/2 charge and 1C discharge in the cutoff voltage range of 2.8-4.4 V and 1C = 200 mAh g^{-1} based on the weight of the NMC811 active material.

As shown in Figure S5a for the Li||NMC811 half cells, similar initial charge/discharge curves are obtained in the formation cycle at C/20. When increasing the charge rate to C/2 and discharge rate to 1C, the highest overpotential is observed for the LHCE of LiFSI/TEPa-BTFE system (Figure

S5b). All the four flame-retarding or nonflammable electrolytes show improved capacity retention in the 50 cycles compared to the control electrolyte (Figure S5c). It should be noticed that the capacity fading in Figure S5c is possibly also related to the side reactions of the electrolyte with Li metal on Li anode side. As shown in Figure S5d, the two LHCEs LiFSI/TEPa-BTFE and LiFSI/TEPa-EC-BTFE have the highest CE close to 100% during the cycling.

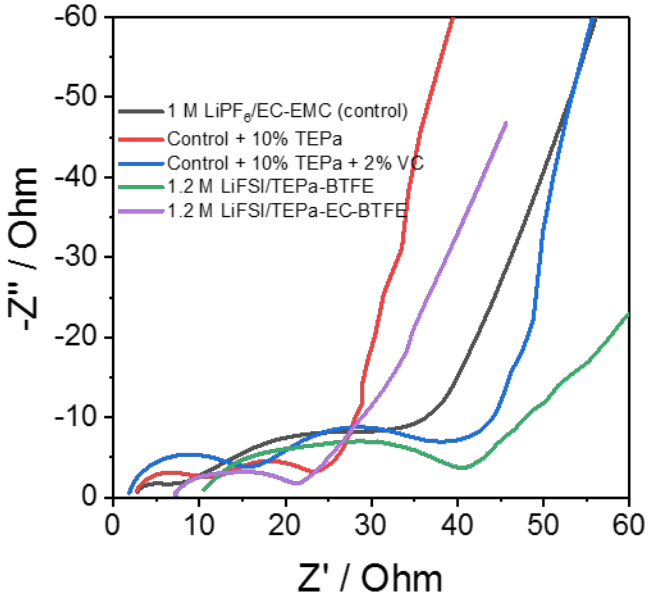

Figure S6. EIS spectra obtained from Gr||NMC811 cells with the five electrolytes after 2 formation cycles at C/20.

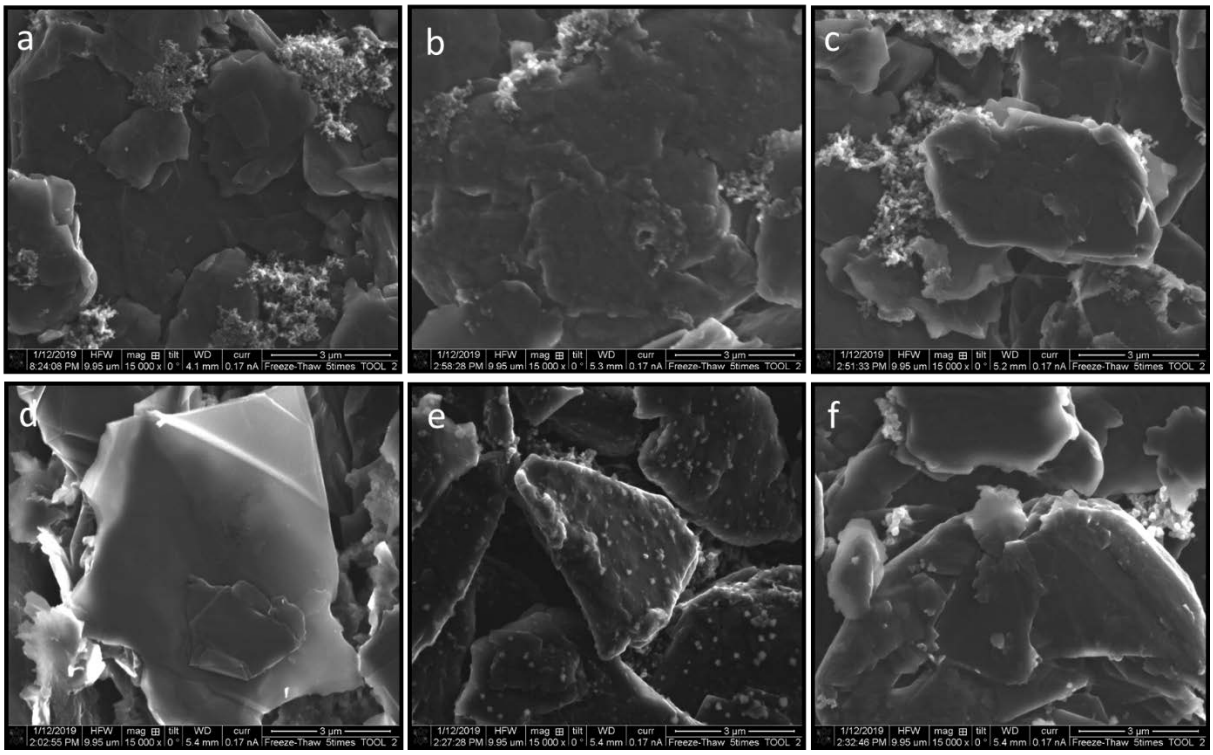

Figure S7. SEM images of the (a) pristine graphite and (b-f) collected Gr anodes cycled in Gr||NMC811 cells with five different electrolytes for 50 cycles. (b) 1 M $LiPF_6$/EC-EMC (control), (c) control + 10% TEPa, (d) control + 10% TEPa + 2% VC, (e) 1.2 M LiFSI/TEPa-BTFE and (f) 1.2 M LiFSI/TEPa-EC-BTFE.

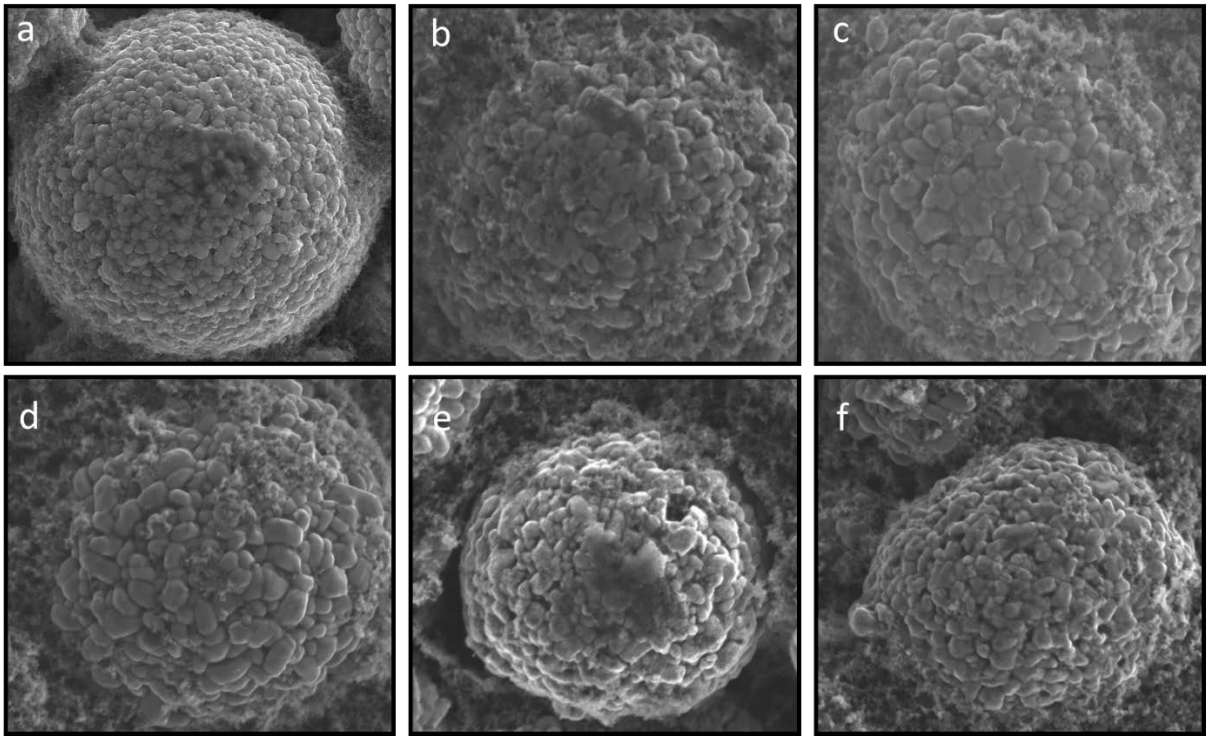

Figure S8. SEM images of the (a) pristine NMC811 cathode and (b-f) collected NMC811 cathodes cycled in Gr||NMC811 cells with five different electrolytes for 50 cycles. (b) 1 M $LiPF_6$/EC-EMC (control), (c) control + 10% TEPa, (d) control + 10% TEPa + 2% VC, (e) 1.2 M LiFSI/TEPa-BTFE and (f) 1.2 M LiFSI/TEPa-EC-BTFE.

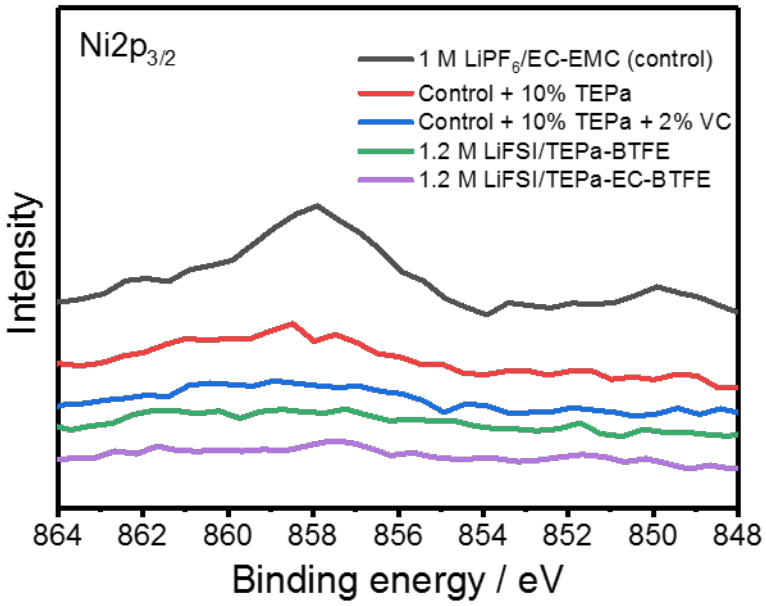

Figure S9. Ni 2p XPS spectra of Gr anodes obtained from Gr‖NMC811 cells with the five electrolytes after 50 cycles.

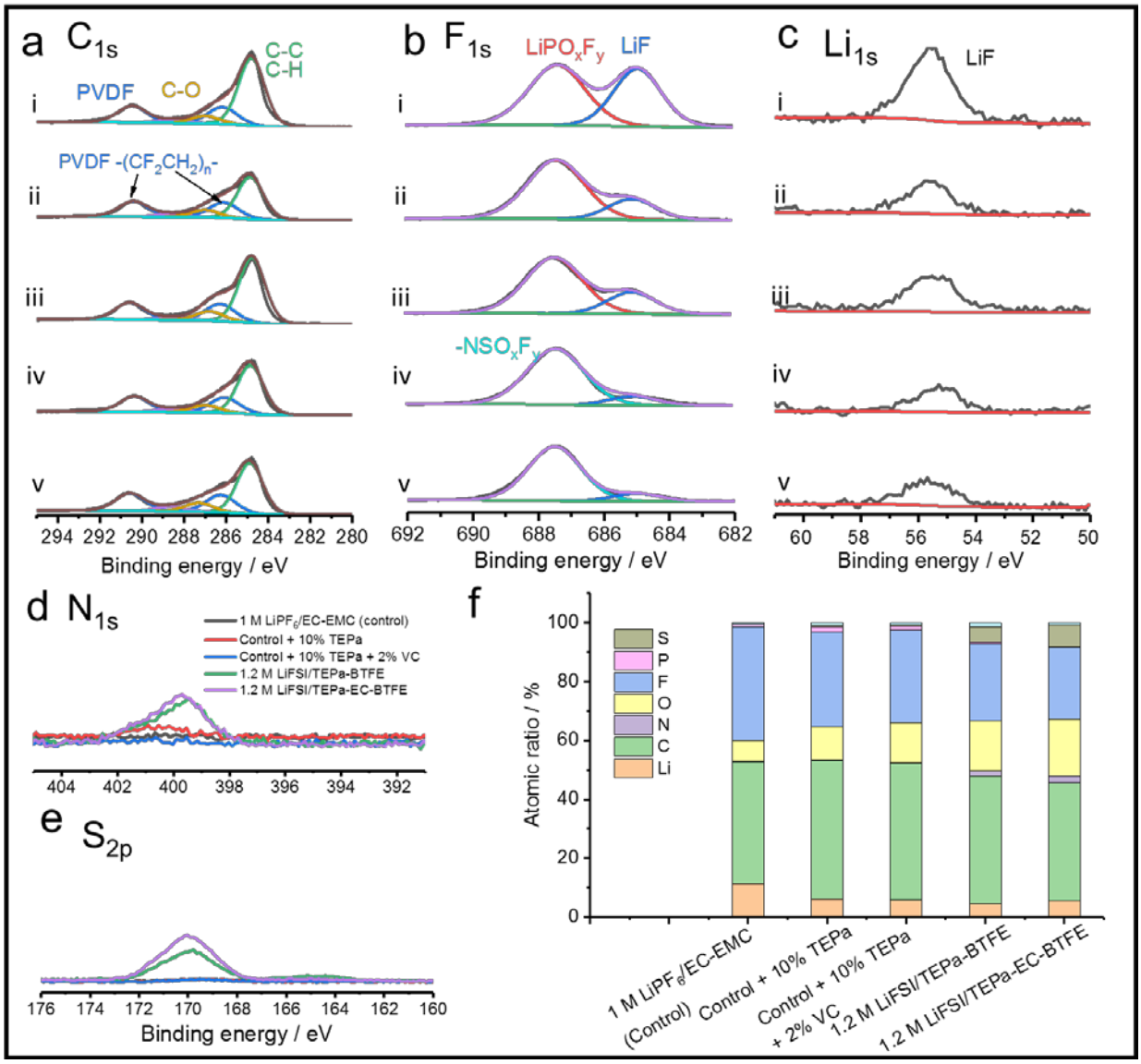

Figure S10. Surface passivation chemistry on NMC811 cathodes after 50 cycles given by XPS results of (a) C 1s, (b) F 1s, (c) Li 1s, (d) N 1s and (e) S2p spectra. The spectra from top to bottom in (a) - (c) are in the sequence of (i) 1 M $LiPF_6$/EC-EMC (control), (ii) control + TEPa, (iii) control + TEPa + VC, (iv) 1.2 M LiFSI/TEPa-BTFE and (v) 1.2 M LiFSI/TEPa-EC-BTFE. (f) Atomic ratio of the elemental distribution on the cycled NMC811 cathodes after 50 cycles in Gr||NMC811 cells with five different electrolytes.

REFERENCES

1. Xu, K.; Ding, M. S.; Zhang, S.; Allen, J. L.; Jow, T. R., Evaluation of Fluorinated Alkyl Phosphates as Flame Retardants in Electrolytes for Li-Ion Batteries: I. Physical and Electrochemical Properties. *J. Electrochem. Soc.* **2003,** *150*, A161-A169.

2. Zou, L.; Liu, Z.; Zhao, W.; Jia, H.; Zheng, J.; Yang, Y.; Wang, G.; Zhang, J.-G.; Wang, C., Solid–Liquid Interfacial Reaction Trigged Propagation of Phase Transition from Surface into Bulk Lattice of Ni-Rich Layered Cathode. *Chem. Mater.* **2018,** *30*, 7016-7026.

3. Li, Y.; Li, Y.; Pei, A.; Yan, K.; Sun, Y.; Wu, C.-L.; Joubert, L.-M.; Chin, R.; Koh, A. L.; Yu, Y.; Perrino, J.; Butz, B.; Chu, S.; Cui, Y., Atomic structure of sensitive battery materials and interfaces revealed by cryo–electron microscopy. *Science* **2017,** *358*, 506-510.

4. Chen, S.; Zheng, J.; Yu, L.; Ren, X.; Engelhard, M. H.; Niu, C.; Lee, H.; Xu, W.; Xiao, J.; Liu, J.; Zhang, J.-G., High-Efficiency Lithium Metal Batteries with Fire-Retardant Electrolytes. *Joule* **2018,** *2*, 1548-1558.

5. Jia, H.; Zou, L.; Gao, P.; Cao, X.; Zhao, W.; He, Y.; Engelhard, M. H.; Burton, S. D.; Wang, H.; Ren, X.; Li, Q.; Yi, R.; Zhang, X.; Wang, C.; Xu, Z.; Li, X.; Zhang, J.-G.; Xu, W., High-Performance Silicon Anodes Enabled By Nonflammable Localized High-Concentration Electrolytes. *Adv. Energy Mater.* **2019,** *9*, 1900784.

6. Ren, X.; Chen, S.; Lee, H.; Mei, D.; Engelhard, M. H.; Burton, S. D.; Zhao, W.; Zheng, J.; Li, Q.; Ding, M. S.; Schroeder, M.; Alvarado, J.; Xu, K.; Meng, Y. S.; Liu, J.; Zhang, J.-G.; Xu, W., Localized High-Concentration Sulfone Electrolytes for High-Efficiency Lithium-Metal Batteries. *Chem* **2018,** *4*, 1877-1892.

7. Xu, K., Nonaqueous Liquid Electrolytes for Lithium-Based Rechargeable Batteries. *Chemical Reviews* **2004,** *104* (10), 4303-4418.